RC22820 (W0306-087) June 17, 2003
Materials Science

IBM Research Report

THE STRUCTURE OF LOW-k TO EXTREME LOW-k SiCOH DIELECTRICS – FTIR CHARACTERIZATION

Alfred Grill, Deborah Neumayer
IBM Research Division
Thomas J. Watson Research Center
P.O. Box 218
Yorktown Heights, NY 10598

Research Division
Almaden - Austin - Beijing - Delhi - Haifa - India - T. J. Watson - Tokyo - Zurich

THE STRUCTURE OF LOW-k TO EXTREME LOW-k SiCOH DIELECTRICS – FTIR CHARACTERIZATION

Alfred Grill and Deborah A. Neumayer
IBM T. J. Watson Research Center, Yorktown Heights, NY 10598

ABSTRACT

Carbon doped oxide dielectrics comprised of Si, C, O, and H (SiCOH) have been prepared by plasma enhanced chemical vapor deposition (PECVD) from mixtures of tetramethylcyclotetrasiloxane (TMCTS) and an organic precursor. The films have been analyzed by determining their elemental composition and by Fourier transform infrared spectroscopy (FTIR) with deconvolution of the absorption peaks. The analysis has shown that PECVD of TMCTS produces a highly-crosslinked networked SiCOH film. Dissociation of TMCTS appears to dominate the deposition chemistry as evidenced by the multitude of bonding environments and formation of linear chains and branches. Extensive crosslinking of TMCTS rings occurs through Si-Si, Si-CH_2-Si, Si-O-Si, and Si-CH_2-O-Si moieties.

The films deposited from mixtures of TMCTS and organic precursor incorporate hydrocarbon fragments into the films. This incorporation occurs most probably through the reaction of the organic precursor and the Si-H bonds of TMCTS. Annealing the SiCOH films deposited from TMCTS and organic precursor results in a large loss of carbon and hydrogen from the films resulting from the fragmentation and loss of the incorporated organic component. The deconvolution of the Si-O-Si asymmetric stretching band of the annealed films shows the existence of a larger fraction of a cage structure and a correspondingly smaller fraction of a networked (highly crosslinked) structure in the SiCOH films deposited from mixtures of TMCTS with organic precursor relative to the films deposited from TMCTS only. The evolution of the volatile hydrocarbon fragments during annealing results in the formation of nanopores and subsequent reduction of the dielectric constants of the films to extreme low-k values.

INTRODUCTION

The replacement of the oxide dielectric in ULSI devices with a low dielectric constant (k) material has been delayed continuously and has caused outward revisions in time of the International Technology Roadmap for Semiconductors (ITRS) projections since 1997. The 2001 ITRS pushed out again low-k dielectric milestones, decelerating advances to ultralow-k dielectrics (k=1.6-2.2) from 2005 to 2009 [1]. The current "low-k" dielectric is fluorosilicate glass (FSG), which has a k value of about 3.5, only slightly lower than that of the silicon dioxide. The main contenders among the PECVD low-k dielectrics with values of k<3 are amorphous materials from the group comprised of Si, C, O, and H which are deposited in conventional PECVD tools [2] and are known by different names, including SiCOH, SiOCH, carbon-doped oxides (CDO), organosilicate glasses (OSG), silicon-oxicarbides, and several trade names given by the various

suppliers who provide processes and tooling for these films. Throughout this paper we will use the term SiCOH to refer to the investigated films.

We have reported elsewhere [3-6] that it is possible to reduce the dielectric constants of SiCOH materials to values as low as k = 2.05, indicating the potential extendibility of PECVD dielectrics to several generations of ULSI chips. The dielectric constant is reduced by adding an organic precursor to the SiCOH precursor, thus incorporating organic fragments in the film, and annealing the deposited films to remove unstable organic fractions from it. Various amounts of porosity are created in the films through this process [7], enabling the adjustment of the dielectric constant at any value between 2.8 and 2.05 by changing the concentration of the organic precursor in the gas feed to the plasma [3, 4, 6]. The present paper intends to shed light in the understanding of the structure of the entire range of SiCOH dielectrics using compositional and FTIR analysis.

EXPERIMENTAL

The SiCOH films were deposited on Si (100) wafers using tetramethylcyclotetrasiloxane (TMCTS, $[MeHSiO]_4$, D_{4h}, $Si_4C_4H_{16}O_4$) as the precursor [2]. 'Me' will be used throughout the paper to denote the methyl radical ($-CH_3$). Helium was used to carry the TMCTS into a parallel plate PECVD reactor where the plasma was sustained by a 13.56 MHz RF power supply. The films with reduced-k values were prepared by admixing an organic precursor (denoted as CH2 in the following) to the TMCTS + He gas feed and annealing the films afterwards in an inert ambience at 400 ^oC [3]. The annealing removes thermally unstable organic fragments and creates porosity in the material. All results are presented for annealed films unless specified otherwise.

The SiCOH films were characterized by Rutherford backscattering (RBS) in combination with forward recoil elastic scattering (FRES) to determine their atomic composition. The FTIR spectra were recorded with a Nicolet Nexus 670 spectrometer using DTGS KBR detector and KBR beam splitter for mid-IR (4000-400 cm^{-1}) data collection. The background for each spectrum was a piece of uncoated wafer that the ensuing films were deposited on. To minimize fringing effects and internal reflections, background and spectra were collected at ~30^o angle from the incident beam. Deconvolution of FTIR peaks was done using the "fit multiple peak Gaussian function" of Origin 6.0 software. More details on the preparation and characterization of the SiCOH films can be found elsewhere [2-6].

RESULTS AND DISCUSSION

It has been shown previously [4] that the dielectric constant of the annealed SiCOH films decreases with increasing fraction of organic precursor in the gas feed, as shown in Figure 1. The SiCOH film grown with TMCTS only, had a dielectric constant of 2.8. For sufficient dilution of the TMCTS precursor the dielectric constant reached a value of 2.05. The entire range of SiCOH films, with k = 2.8–2.05, is characterized by low leakage currents of about 10^{-9} A/cm^2 at 1MV/cm [4] and relatively low coefficients of thermal expansion of about $12x10^{-6}/^oK$ [5]. The hardness and elastic modulus of the SiCOH films decrease with decreasing dielectric constant [5]. It has further been shown

[7] that the decrease of the dielectric constant is directly related to the decrease of the density of the films caused by the formation of porosity in the structure, as shown in Table I. These results indicate that the dielectric constant of the SiCOH films is controlled mainly by the porosity induced in the films and it is of interest to understand how this correlates with the structure of the films.

Film Composition

The elemental concentration ratios are plotted in Figure 2 as a function of the CH2/TMCTS ratio in the gas feed to the plasma, for as deposited and annealed SiCOH films. In the SiCOH film grown from TMCTS only (CH2/TMCTS = 0) the ratio C/Si =1 is the same as in the TMCTS precursor. However, the O/Si ratio in the film is higher and the H/Si ratio is much lower than in the TMCTS precursor. The explanation for the differences in composition between film and precursor will be provided latter. Annealing of the as-deposited SiCOH film grown from TMCTS only results in a slight additional loss of H from the film.

In the as deposited SiCOH films grown with the addition of the organic precursor to TMCTS at a flow ratio in the gas feed of CH2/TMCTS = 0.2 the C/Si and H/Si ratios increase significantly as compared to those in the SiCOH film grown from TMCTS only. As the CH2/TMCTS gas ratio increases, the H/Si ratio decreases but the C/Si ratio remains unchanged, within experimental errors.

Large decreases in C/Si and H/Si ratios are observed after annealing the SiCOH films grown from mixtures of TMCTS with the organic precursor. After annealing the film deposited at a ratio CH2/TMCTS = 0.2, nearly half of the C and H in the as-deposited film is lost, but the O/Si ratio remains unchanged. Furthermore, the C/Si, O/Si and H/Si elemental ratios are unchanged, within experimental error, for the annealed films when the CH2/TMCTS flow ratio is increased form 0.2 to 0.5.

FTIR Analysis

Structural characterization of amorphous films is extremely difficult and we used Fourier transform infrared (FTIR) spectroscopy in the present study to characterize the different bonding arrangements in the SiCOH films. Figure 3 presents the FTIR spectra of the TMCTS precursor and of several as-deposited and annealed films. The peak assignments are listed in Table II for TMCTS and for annealed SiCOH films grown from TMCTS only (k=2.8) and from TMCTS plus organic precursor (k=2.05). The detailed justification for the peak assignments is provided in Appendix A. As shown in Figure 3a, the FTIR spectra of the TMCTS precursor consists of a number of sharp absorptions consistent with a well defined molecular structure. The peak assignment is straightforward and is summarized in Table 2.

The FTIR spectrum of the annealed SiCOH film grown from TMCTS only (Figure 3b) has broader peaks than the FTIR spectrum of TMCTS, indicating a less defined molecular structure in the film. Additionally, the FTIR absorption peaks of the film have shifted to slightly higher wave numbers and new absorptions are observed. Specifically, in the C-H stretching absorption region, new absorptions at 2916 cm^{-1} with a shoulder at 2880 cm^{-1} are observed and attributed to stretching of C-H in CH_2. Concurrently, the Si-H stretching absorption has shifted to a slightly higher wavenumber at 2178 cm^{-1} and a new Si-H stretching absorption is observed at 2234 cm^{-1}. The absorption at 2234 cm^{-1}

has been attributed to a bonding arrangement in which the hydrogen is bonded as H-SiO_3. [8-14]. A new weak absorption at 1358 cm^{-1} is observed and assigned to bending of C-H in Si-CH_2-Si crosslinks [15-19]. The Si-CH_3 bending deformation has shifted to a higher wavenumber at 1273 cm^{-1} and broadened, which might indicate the formation of $SiMe_3$ groups [18].

The Si-O-Si asymmetric stretching band of the SiCOH film at 1250-950 cm^{-1} has broadened compared to the peak in TMCTS, increased in relative intensity, and appears to have a peak at 1047 cm^{-1} with a shoulder at a larger wavelength. However, the Si-O-Si peak of the SiCOH film cannot be deconvoluted in two peaks, but instead has to be deconvoluted into three peaks centered at 1135, 1063, and 1023 cm^{-1} as illustrated in Figure 4a [6]. The peak at 1135 cm^{-1} is attributed to larger angle Si-O-Si bonds in a cage structure with a bond angle of approximately 150 ^{o} [11-13, 20]. The peak at 1063 cm^{-1} is assigned to the stretching of smaller angle Si-O-Si bonds in a network structure. Some contribution to this absorption may also come from intact TMCTS rings preserved in the SiCOH film (see first column in Table II). The peak at 1023 cm^{-1} can be assigned to stretching of even smaller Si-O-Si bond angle, such as might be encountered in a networked silicon suboxide [21-23]. Some contribution to this absorption may also come from bound six-membered $[H_xMe_{2-x}SiO]_3$ rings contained in the SiCOH film [16, 17].

The Si-O-Si asymmetric stretching band frequency shifts are attributed to changes in the Si-O-Si bonding angle. In fully relaxed stoichiometric thermal silicon oxides grown at temperatures >1000 ^oC, the bonding angle is reported to be ~144^o with an FTIR absorption around 1080 cm^{-1}. However, in low temperature stoichiometric silicon oxides, the FTIR stretching frequency has been shown to decrease from 1080 to 1060 cm^{-1} as the Si-O-Si bond angle decreases [21]. In silicon suboxides, a decrease in the frequency of the Si-O-Si asymmetric stretching vibration has also been observed and attributed to the silicon atoms having one or more non-oxygen neighbors [21, 22] (see Appendix A). Thus, the Si-O-Si asymmetric stretching mode frequency shift is attributed to variations of bond angles and the broadening of the band is a manifestation of a statistical distribution of different bonding arrangements at each silicon atom site.

While the SiCOH film may contain C-O-C or Si-O-C bonds, any contributions to the absorptions at 1200-1000 cm^{-1} from C-O-C, or Si-O-C asymmetric stretching vibrations cannot be identified because they overlap with the Si-O-Si asymmetric stretching band [18, 24, 25].

The broad absorption band between 950-650 cm^{-1} is deconvolutable into 5 peaks centered at 892, 840, 802, 774, and 736 cm^{-1} (Figure 5a). The peaks in this region are attributable to H-Si-O and Si-Me_x (x = 1, 2, or 3) vibrations, which overlap each other making definitive and qualitative assignments difficult. Nevertheless, as explained in Appendix A, the major contribution to the band at 890 cm^{-1} in the SiCOH film deposited from TMCTS only can be attributed to H-Si-O bond bending in which each silicon atom has three oxygen neighbors [8-13].

The broad band at 848 cm^{-1} observed in our films is most likely composed of overlapping vibrations from H-Si-O, $SiMe_3$ and $SiMe_2$ with H-Si-O and $SiMe_3$ as the major contributors (see Table II). The observation of the absorption at 848 cm^{-1}, which is at least partially attributable to $SiMe_3$ end groups, suggests the existence of some linear chains in the SiCOH film. However, because we cannot qualitatively separate out the $SiMe_3$ contribution in the FTIR spectrum, due to overlapping contributions from H-Si-O,

and $SiMe_x$, we cannot estimate the relative ratio of linear chains to ring structures in the film.

The absorption band at 802 cm^{-1} is attributed to $SiMe_2$ vibrations, the band at 774 cm^{-1} to $SiMe_1$ and the weak band at 736 cm^{-1} to Si-O-Si symmetric stretching. The absorption band at 440 cm^{-1} is attributed to bond bending of networked Si-O-Si and to ring opening vibrations [11-13]. Si-Si stretching vibrations have also been reported in the 400-550 cm^{-1} range [26].

The as deposited SiCOH films with lower k values, prepared with the addition of organic precursor to TMCTS, are characterized by a strongly increased peak intensity in the 3100-2700 cm^{-1} region (C-H_i stretching vibrations), an absence of Si-H vibrations in the 2400-2000 cm^{-1} region, and reduced intensity of the 890 and 848 cm^{-1} absorptions (H-Si-O bending and $SiMe_x$ vibrations), compared to the films deposited from TMCTS only, as shown in Figure 3c. The new absorptions at 2932 (CH_2 stretch) and 1461 cm^{-1} (CH_2 bend, free of silicon) and the increased relative absorption of the CH_2 stretch at 2875 cm^{-1} are the result of the incorporation of organic components in the as deposited SiCOH films. The sharp reduction of Si-H peak intensity suggests that the organic precursor is reacting with the Si-H bonds in TMCTS during the formation of the film. The doublet centered at 1740 and 1714 cm^{-1}, observed in the as-deposited reduced-k SiCOH films, can be assigned to C=O stretching in the film.

As shown in Figure 3d, the annealing of the as-deposited reduced-k SiCOH film reduces the C-H_x stretching vibrations (3100-2700 cm^{-1}) and CH_2 bend (1461 cm^{-1}) peak intensities. The doublet centered at 1740 and 1714 cm^{-1} disappears after annealing.

In the annealed reduced-k SiCOH film, the Si-O-Si asymmetric stretching band has split into an apparent doublet. Deconvolution of this band yields three peaks at 1140, 1063 and 1035 cm^{-1}. The cage Si-O-Si peak of the film with k=2.05 has shifted to slightly higher wavenumbers, at 1140 cm^{-1}, and increased in relative area compared to that of SiCOH films deposited with TMCTS only. The silicon suboxide peak has also shifted to a slightly higher wavenumber at 1035 cm^{-1}.

The broad band between 950-650 cm^{-1} in the annealed reduced-k SiCOH film has decreased in intensity relative to the annealed SiCOH film grown from TMCTS only. Deconvolution of this band yields 5 peaks at 904, 837, 804, 777 and 726 cm^{-1}. Notably, the absorption at 904 cm^{-1}, attributed primarily to H-Si-O bonds, is negligible in the reduced-k SiCOH film as shown in Figure 5b. This is consistent with the absence of absorptions attributable to Si-H in the reduced-k SiCOH films grown with the addition of the organic precursor. The absorption at 837 cm^{-1}, attributable to H-Si-O and $SiMe_3$, has also decreased in peak intensity. The major contributor to this peak in the annealed reduced-k SiCOH films with no Si-H absorptions is assumed to be $SiMe_3$. The peak at 804 cm^{-1} assigned to $SiMe_2$ has decreased in peak intensity. The peak at 777 cm^{-1} has also decreased in intensity and the FWHM has decreased indicating a smaller contribution from $SiMe_3$.

The observations discussed above are summarized for the entire range of the investigated films in Table III and Figures 6-8. Table III presents the integrated peak areas for the annealed films. The scatter of the values shown in Figures 6-8 are caused by experimental errors and errors in the deconvolution calculations. As shown in Figure 6, the peak area ratio of CH_i /$SiCH_3$ (at 1275 cm^{-1}) increases sharply with the addition of the organic precursor to TMCTS, due to the incorporation of organic precursor in the SiCOH film. However, the CH_i/$SiCH_3$ peak ratio decreases as the CH2 /TMCTS ratio increases and the dielectric constant decreases (Figure 6a). This may be caused by the increasing

porosity of the film as the CH2/TMCTS ratio is increased. Concurrently, the SiH/$SiCH_3$ area ratio in the films decreases sharply with the introduction of the organic precursor, due to the incorporation of organic fragments in the SiCOH film at Si-H groups (Figure 6f). A corresponding decrease in the HSiO (at 890 cm^{-1})/$SiCH_3$ area ratio is observed (Figure 6b), consistent with the loss of Si-H groups in the reduced-k films grown with the addition of the organic precursor. The persistence of the absorption at 848 cm^{-1} (Figure 6c) even in films with no observable Si-H absorptions is an indication of the existence of some linear branches and/or chains in the films. Interestingly, the $SiMe_2$/$SiCH_3$ peak area ratio (Figure 6d) decreases with decreasing dielectric constant and the $SiMe_1$/$SiCH_3$ peak area ratio increases (Figure 6e), indicating greater retention of the TMCTS ring structure in the films.

The peak area ratio of the $SiCH_3$ (1275 cm^{-1})/SiO (total absorption from 1200-1000 cm^{-1}) is often used to qualify SiCOH films. Within experimental error, the Si-CH_3/SiO area ratio in our films is the same for films grown with TMCTS only and for films grown with TMCTS and organic precursor. Figure 2 showed that the films deposited from the mixtures of TMCTS and organic precursor contain significantly higher amounts of C and H than the films deposited from pure TMCTS, therefore one might expect this to be reflected in significantly higher $SiCH_3$/SiO area ratios. As this is not the case, it has to be assumed that the CH_x fractions added to the films are not connected in Si-CH_3 bonds. This is consistent with the incorporation of the organic fragments by substitution at the Si-H sites as discussed before. Furthermore, the Si-CH_3/SiO intensity ratios are the same, within experimental errors, for the as-deposited and the annealed films grown with TMCTS and organic precursor, in spite of the fact that a large amount of carbon and hydrogen are lost from the films during annealing. This can be explained by preferential loss of hydrocarbon fragments from the incorporated organic fraction and preferential retention of Si-CH_3 ligands during annealing.

The peak area ratio of SiOSi-cage/SiOSi-network absorptions increases with decreasing dielectric constant, as shown in Figure 7, indicating that the addition of organic precursor has contributed to the enhancement of the cage structure. The formation of the cage structure is consistent with increasing porosity shown in Table 1. In the same time the peak area ratio of silicon suboxide/SiOSi-network decreases with increasing addition of organic precursor.

The FWHM values of the deconvoluted SiO peaks are presented in Figure 8, which shows that the FWHM of the network and silicon suboxide Si-O-Si peaks decrease, while that of the cage Si-O-Si peak increases with decreasing dielectric constant. The increase in the cage Si-O-Si peak's FWHM might be attributable to an increasing variety of bonding environments in the cage structure. The decrease in the network and silicon suboxide Si-O-Si peak's FWHM can be attributed to a less variable network and silicon suboxide Si-O-Si bond angle in the reduced-k SiCOH film.

Film formation and structure

The FTIR spectra of the SiCOH films deposited from TMCTS only indicate that the films are highly-crosslinked complex materials, primarily composed of a network structure formed by a mixture of different bonding arrangements in cyclic and some linear branch structures. Based on the analysis of the FTIR spectra presented above, the structure of these films can be described by the diagram shown in Figure 9. An attempt to summarize the reaction pathways leading to the deposition of the films and the different

bonding arrangements is presented next. A description of the potential reactions resulting in the formation of the films is given in Appendix B.

The most probable reactions to occur in the plasma are those involving the breaking of the weakest bonds of the TMCTS precursor. However, due to the distribution of electron energies in the plasma, one would expect partial dissociation of higher-energy bonds as well. As summarized in Table IV [27], the weakest and most reactive bond of TMCTS is the Si-H bond. Therefore, the most likely reaction leading to the formation of SiCOH films from TMCTS only (k =2.8) is hydrogen abstraction, yielding an ionized TMCTS ring (reaction 1 of Scheme 1 in Appendix B). Other probable reactions are depicted in Scheme 1 in Appendix B and include methyl abstraction (reaction 2), loss of H from the Si-CH_3 ligand (reaction 3), cleavage of Si-O bond to form a linear diradical (reaction 4), ring decomposition yielding $[HMeSiO]_3$ (D_{3h}) via loss of methylsilanone $CH_3HSi=O$ (D_{1h}) (reaction 5) [15-17, 28, 29], ring enlargement and contraction reactions (reaction 6) [16, 17, 19, 30], and formation of linear chains and branches via cleavage of Si-O bonds by ionized TMCTS radicals (reaction 7). The structure of the resulting SiCOH film is therefore highly complex and likely comprised of a variety of different crosslinked environments as illustrated in Figure 9. Scheme 2 in Appendix B depicts the paths to the formation of Si-Si, Si-CH_2-Si, Si-O-Si, and Si-O-CH_2-Si crosslinks through reactions 8, 9, 10 and 11, respectively. All these reactions have the potential to take place in the plasma.

However, the loss of hydrogen and increased concentration of oxygen, the broadness of the peaks in the FTIR spectrum, observation of an intense FTIR absorption at least partially attributable to $SiMe_3$, and lack of resemblance of the film FTIR spectrum to the TMCTS FTIR spectrum, indicate that complete ring fragmentation occurs to a large extent in the plasma, leading to the deposition of SiCOH films from TMCTS only. Similar dissociation of the precursor in the plasma has been reported for hexamethyldisiloxane (HMDS), hexamethylcyclotrisiloxane (HMCTS), and octamethylcyclotetrasiloxane (OMCTS) [15, 16, 19].

The increased oxygen content in the SiCOH film relative to that in the TMCTS precursor may be explained by the loss of more volatile $SiMe_xH_y$ species resulting from the fragmentation of the TMCTS ring . From elemental analysis data we would expect $y>>x$ in the volatile $SiMe_xH_y$ species because the C/Si ratio is retained and the H/Si ratio is halved relative to the TMCTS monomer. If the reaction was driven to completion as shown below, SiO_2 would be formed.

$$[HSiMeO]_4 \longrightarrow 2\ SiMe_{4-x}H_x + 2\ SiO_2$$

Fragmentation of TMCTS and loss of $SiMe_xH_y$ species is similar to the observation of low molecular weight species during GC/MS studies of plasma polymerization of OMCTS [19]. Additionally, loss of SiH_4 has been observed during thermal annealing of HSQ [31].

The addition of the organic precursor to the plasma feed results in increased carbon and hydrogen content relative to Si, increased porosity, and reduced dielectric constant of the resultant SiCOH films. Based on the FTIR analysis, the structure of these films can be described by the diagram shown in Figure 10. While the basic reactions leading to the formation of the films are similar to those described above, the lack of evidence of Si-H groups in the FTIR spectra of the as-deposited SiCOH films grown from TMCTS with organic precursor and the increased peak intensity of absorptions attributable to CH_i

(3100-2700 cm-1) indicate that the incorporation of the organic fractions in the film occurs preferentially at the Si-H sites. The incorporation of the organic fractions appears to promote the formation of cage structure in the SiCOH film as evidenced by the intense FTIR absorption at 1140 cm^{-1} attributable to the cage structure.

Significant loss of C and H is observed after annealing the SiCOH films deposited from TMCTS and organic precursor. This loss is most likely attributable to the fragmentation and loss of organic fractions incorporated in the reduced-k films. The loss of the hydrocarbon fragments during annealing leads to increased porosity in the annealed reduced-k SiCOH films. This loss is consistent with the reduction of the peak intensity of the CHx absorptions at 3100-2700 cm^{-1}, and the CH_2 (free of Si) absorption at 1461 cm^{-1} in the FTIR spectra of annealed films compared with as deposited films.

CONCLUSIONS

FTIR and elemental analysis of SiCOH films show that the PECVD of TMCTS produces a randomly highly crosslinked networked SiCOH film. The dissociation of TMCTS in the plasma dominate the deposition chemistry as evidenced by the multitude of bonding environments and formation of linear chains and branches in the films. Crosslinking occurs through Si-Si, Si-O-Si, Si-CH_2-Si, and Si-CH_2-O-Si moieties. Increased oxygen content in the films is proposed to result from the fragmentation of TMCTS, and preferential loss of non oxygen containing $SiMe_{4-x}H_x$ species.

The films deposited from mixtures of TMCTS with organic precursor incorporate organic fractions in the film. The incorporation of the organic components takes place through the reaction of the organic precursor with Si-H. From the deconvolution of the Si-O-Si asymmetric stretching band, we have demonstrated a larger percentage of a cage structure and a smaller percentage of a networked (or highly crosslinked) structure in the SiCOH films deposited from TMCTS with organic precursor relative to the films deposited from TMCTS only. Annealing the SiCOH film deposited from TMCTS with organic precursor results in a large loss of carbon and hydrogen from the film, due to fragmentation and loss of incorporated organic fragments. The loss of the volatile organic fragments during annealing results in the formation of nanopores and subsequent reduction of the dielectric constant of the films to extreme low-k values.

REFERENCES

1. 2001 International Technology Roadmap for Semiconductors, Interconnects.
2. A. Grill, L. Perraud, V. Patel, C. Jahnes, and S. Cohen, Mat. Res. Soc. Symp.Proc., **565**, 107 (1999).
3. A. Grill and V. Patel, Mat. Res. Soc. Symp. Proc., **612,** D2.9.1 (2000).
4. A. Grill and V. Patel, Appl.Phys.Lett., **79,** 803 (2001).
5. A. Grill, D. Edelstein and V. Patel, Conference Proceedings (MRS) **ULSI XVII,** 253 (2002).
6. A. Grill, J.Appl.Phys., **93** (2003) 1785.
7. A. Grill, V. Patel, K.P. Rodbell, E. Huang and S. Christiansen, Characteristics of low-k and ultralow-k PECVD deposited SiCOH films, Mat. Res. Soc. Symp. Proc. Vol. **716,** 569 (2002).

8. G. Lucovsky, J. Yang, S.S. Chao, J.E. Tyler, W. Czubatyj, Phys Review B 28, 3225 (1983).
9. M. J. Loboda, C. M. Grove, and R.F. Schneider, J.Electrochem.Soc. **145**, 2861 (1998)
10. M. G. Albrecht, C. Blanchette, J. Electrochem. Soc. **145**, 4019 (1998).
11. P. Bornhauser, G. Calzaferri, Spectrochimica Acta, **46A**, 1045 (1990).
12. P. Bornhauser, G. Calzaferri, J. Phys. Chem., **100**, 2035 (1996).
13. C. Marcolli, G. Calzaferri, J. Phys. Chem. **101**, 4925 (1997).
14. P.G. Pai, S.S. Chao, Y. Takagi, G. Lucovsky, J. Vac. Sci. Technol. **A4**, 689 (1985).
15. C. Rau, W. Kulisch, Thin Solid Films, **249**, 28 (1994).
16. H.G. Pryce Lewis, D.J. Edell, K.K. Gleason, Chem. Mater. **12**, 3488 (2000).
17. H.G. Pryce Lewis, T.B. Casserly, K.K. Gleason, J. Electrochem. Soc. **148**, F212 (2001)
18. T.R. Crompton, The Chemistry of Organic Silicon Compounds, S. Patai, Z. Rappoport editors, John Wiley&Sons, New York, 416-421 (1989).
19. A.M. Wrobel, M. Kryszewski, M. Gazicki, J. Macromol. Sci.-Chem. **A20,** 583 (1983).
20. L.H. Lee, W.C. Chen, W.-C. Liu, J. Polymer Sci.: Part A Polym. Chem. **40A**, 1560 (2002).
21. P.G. Pai, S.S. Chao, Y. Takagi, G. Lucovsky, J. Vac. Sci. Technol. **A4**, 689 (1986).
22. G. Lucovsky, M.J. Manitini, J.K. Srivastava, E.A. Irene, J. Vac. Sci. Technol. **B5**, 530 (1987).
23. Y.-H. Kim, M.S. Hwang, H.J. Kim, J.Y. Kim, Y. Lee, J. Appl. Phys., **90**, 3367 (2001).
24. N. Wright, M.J. Hunter, J. Am. Chem. Soc., **69**, 803 (1947).
25. S.C. Deshmukh, E.S. Aydil, J. Vac. Sci. Technol., **A13**, 2355 (1995).
26. R. Zink, K. Hassler, Spectrochimica Acta, **A55**, 333 (1999).
27. Handbook of Chemistry and Physics, D.R. Lide editor, **81st edition**, CRC Press: Boca Raton, Fl, 9-52 (2001).
28. I.M.T. Davidson, J.F. Thompson, J. Chem. Soc., Faraday Trans., 7**1**, 2260 (1975).
29. V.N. Khabashesku, Z.A. Kerzina, A.K. Malsev, O.M. Nefedov, J. Organometal. Chem. **364**, 301 (1989).
30. C. Xu, A.S. Borovik, Z. Wang, J. Arno, T.H. Baum, Mat. Res. Soc. Symp. Proc. **716**, B128.1 (2002).
31. V. Belot, R. Corriu, D. Leclercq, P.H. Mutin, A. Vioux, Chem. Mater. 3, 127 (1991).
32. D.C. McKean, I. Torto, Spectrochimica Acta **49A**, 1095 (1993).
33. R.E. Richards, H.W. Thompson, J. Chem.. Soc., 124 (1949).
34. Pauling scale.
35. Aldrich Library of FT-IR spectra, editor is C.J. Pouchert, 1985
36. W.-C. Liu, C.-C. Yang, W.-C. Chen, B.-T. Dai, M.-S. Tsai, J. Non. Cryst. Solids **311**, 233 (2002).

Appendix A: Assignment of IR absorption peaks.

The assignment of the peaks in the 3100-2700 cm^{-1} absorption band to C-H_x stretching vibrations can be found in references [15-18, 32]. The absorption peak at 2165 cm^{-1} corresponds to Si-H vibration [8]. The absorption at 2234 cm^{-1} has been attributed to Si-H in a bonding arrangement in which the hydrogen is bonded as $HSiO_3$. This vibration has been observed in oxygen containing hydrogenated amorphous silicon films [8] and in hydrosilsesquioxanes (HSQ) [9-14]. The absorption at 1358 cm^{-1} is assigned to bending of C-H in Si-CH_2-Si crosslinks [15-19]. The shift of the Si-CH_3 bending absorption to a higher wavenumber than in TMCTS, to 1273 cm^{-1}, and its broadening might indicate the formation of $SiMe_3$ (Me=-CH_3) groups [18].

The Si-O-Si asymmetric stretching band of the SiCOH film at 1250-950 cm^{-1} can be deconvoluted into three peaks centered at 1135, 1063, and 1023 cm^{-1}]. The peak at 1135 cm^{-1} is attributed to larger angle Si-O-Si bonds in a cage structure with a bond angle of approximately 150 ^{o} [11, 13, 20]. The peak at 1063 cm^{-1} is attributed to the stretching of smaller angle Si-O-Si bonds in a network structure. Some contribution to this absorption may also come from preserved intact TMCTS rings in the SiCOH film. The peak at 1023 cm^{-1} is attributed to stretching of even smaller Si-O-Si bond angle such as might be encountered in a networked silicon suboxide [21-23]. Some contribution to this absorption may also come from bound six-membered $[H_xMe_{2-x}\ SiO]_3$ rings in the SiCOH film [16, 17]. The Si-O-Si asymmetric stretching band is offset at 1020 cm^{-1} in tricyclicdimethylsiloxanes [24, 33]. Any contributions to absorptions at 1200-1000 cm^{-1} from C-O-C, or Si-O-C asymmetric stretching [18, 24, 25] overlap with the Si-O-Si asymmetric stretching band.

The Si-O-Si asymmetric stretching band frequency shifts are attributed to changes in the Si-O-Si bonding angle (θ). In fully relaxed stoichiometric thermal silicon oxides, grown at temperatures >1000 ^{o}C, the bond angle is reported to be ~144^o, as shown schematically in Figure 11a, and has an FTIR absorption peak around 1080 cm^{-1}. However, in low temperature stoichiometric silicon oxides, the FTIR stretching frequency has been shown to decrease from 1080 to 1060 cm^{-1} as the Si-O-Si bond angle decreases [21]. In silicon suboxides, a decrease in the frequency of the Si-O-Si asymmetric stretching vibration has also been observed and attributed to the silicon atoms having higher probability of having one or more non-oxygen neighbors [21, 22]. A bonding structure model based on the distortion of SiO_3X tetrahedral due to electronegativity differences has been proposed to explain the change in bonding angle for carbon doped silicon suboxides [23]. The SiO_3X tetrahedral is depicted in Figure 11b, X being an atom such as C, Si or H, which is less electronegative than oxygen. It is theorized that such an atom attracts the bonding electrons in the Si-X bond less strongly than oxygen in the Si-O bond thus distorting the tetrahedra and reducing the bond angle to <144^o.

The electronegativity bonding structure model does not hold true for a HSQ or a methylsilsesquioxane (MSQ) cage structure, where H or C is substituted in the SiO_3X tetrahedral, because even though H and C are less electronegative than oxygen (2.2 eV and 2.55 eV vs. 3.5 eV respectively [34]), the Si-O-Si bond angle is reported to be approximately equal to 150^o [11-13, 20]. Therefore, in the HSQ or MSQ cage structure geometric constraints must play a greater role in determining bond angle than electronegativity. A SiO_3X tetrahedra distorted due to geometric constraints is depicted in Figure 11c. Thus, the Si-O-Si asymmetric stretching mode frequency shift is attributed

to variation of bond angle and the broadening of the band is a manifestation of a statistical distribution of different bonding arrangements at each silicon atom site.

The broad band between 950-650 cm^{-1} is deconvolutable into 5 peaks centered at 892, 840, 802, 774, and 736 cm^{-1} (Figure 5a). The peaks in this region are assigned to H-Si-O and Si-Me_x (x = 1, 2, or 3) vibrations, which overlap each other making definitive and qualitative assignments difficult. The major contribution to the band at 890 cm^{-1} is attributed to H-Si-O bond bending in which each silicon atom has three oxygen neighbors. This assignment has been applied to a band at 885 cm^{-1} for HSQs [9-13] and to a band at 875 cm^{-1} in amorphous oxygen-containing silicon hydrogen alloy films [8]. In SiCOH films deposited from hexamethyldisiloxane (HMDS), octamethylcyclotetrasiloxane (OMCTS), and hexamethylcyclotrisiloxane (HMCTS), a band at 878-895 cm^{-1} has been attributed to the symmetric CH_3 rocking and Si-C stretching vibrations in $SiMe_2$ [15-19], however in these films the band is relatively weak despite the existence of $SiMe_2$ groups in the starting molecule. Therefore, we can assume H-Si-O to be the major contributor to the 890 cm^{-1} absorption in the SiCOH film deposited from TMCTS only.

The broad band at 848 cm^{-1} is attributed to H-Si-O and $SiMe_3$ vibrations. The H-Si-O bending assignment has been applied to a band at 840-857 cm^{-1} for HSQs [9-13] and at 830 cm^{-1} for high molecular weight fractions of HSQs [9, 10]. A band at 850 cm^{-1} has been assigned to a H-SiO_2Si cis configuration in H doped silicon suboxide [8]. A band at 840 cm^{-1} has been assigned to $SiMe_3$ end groups in linear polysiloxanes [26, 24, 33] and in SiCOH films deposited from HMDS, OMCTS and HMCTS [15-19]. A weak band at 858 cm^{-1} has been observed in cyclosiloxanes with only $SiMe_2$ groups [24, 33]. Most likely the band at 848 cm^{-1} observed in our films is composed of overlapping vibrations from H-Si-O, $SiMe_3$ and $SiMe_2$ with H-Si-O and $SiMe_3$ as the major contributors.

The band at 802 cm^{-1} is attributed to $SiMe_2$ vibrations [15-19, 24, 35]. In SiO_2 a weak band at 810 cm^{-1} is attributed to skeletal network Si-O-Si symmetric stretching, and is a possible minor contributor to this band. The band at 774 cm^{-1} is attributed to $SiMe_1$ vibrations, which was observed at 754 cm^{-1} in TMCTS, 780 cm^{-1} in MSQ [36] and at 769-789 cm^{-1} in $SiMe_1(OR)_3$ alkoxysilanes depending on the substituent [24]. Another possible contributor to this band is symmetric CH_3 rocking and Si-C stretching vibrations from $SiMe_3$, which has been observed at 760 cm^{-1} [24, 33]. The weak band at 736 cm^{-1} is attributed to Si-O-Si symmetric stretching [12, 13]. The absorption band at 440 cm^{-1} is attributed to bond bending of networked Si-O-Si and to ring opening vibrations [11-13]. Si-Si stretching vibrations have also been reported in the 400-550 cm^{-1} range [26].

The 1740 and 1714 cm^{-1} peaks are attributed to C=O stretching in the film [15] and the 1461 cm^{-1} absorption peak is attributed to CH_2 bend, free of silicon, vibrations [15, 35].

Appendix B: Potential plasma reactions for the formation of SiCOH films from TMCTS

Scheme 1. Possible dissociation paths of TMCTS

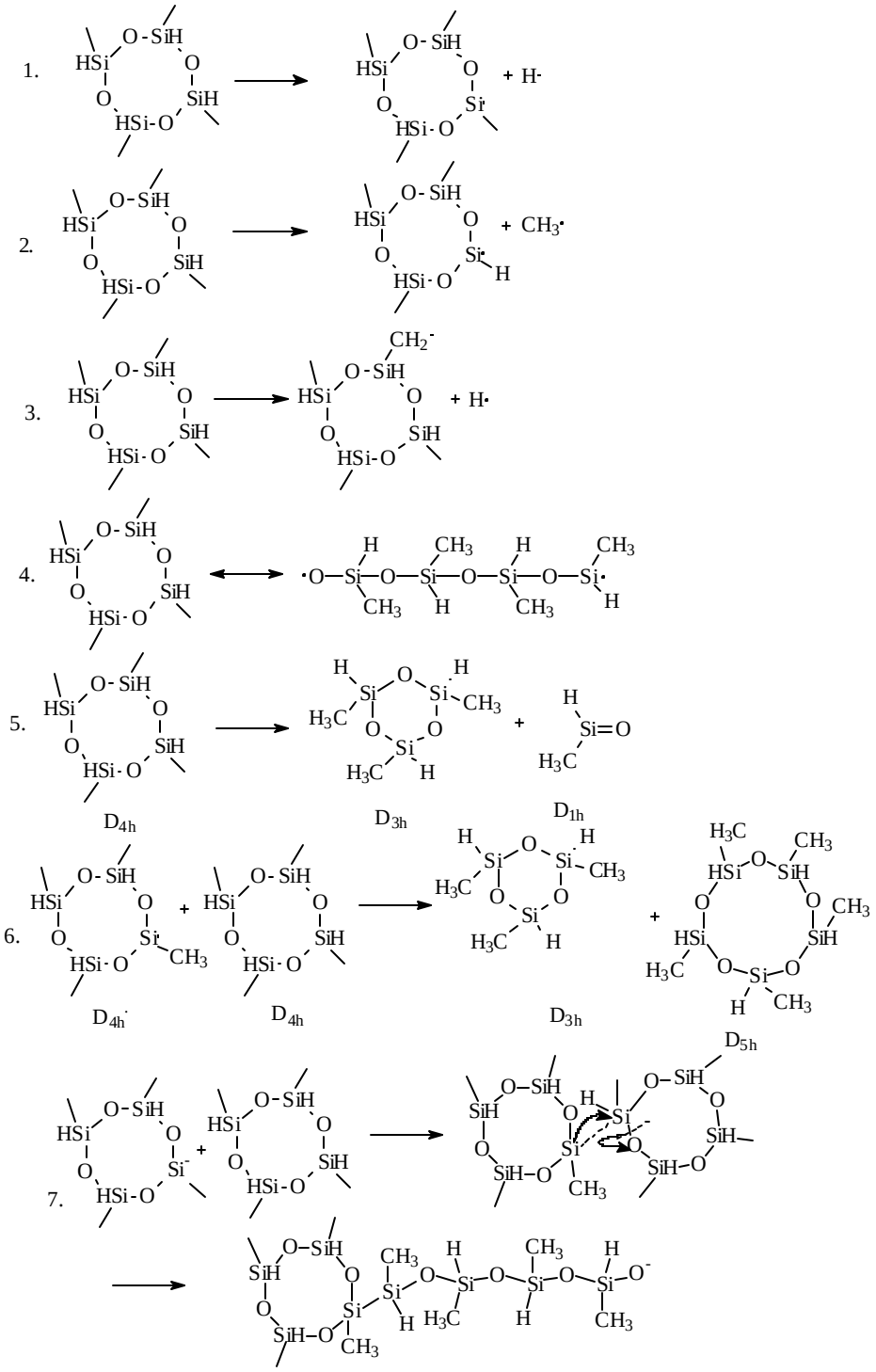

Scheme 2. Crosslinking reaction paths for the TMCTS fragments

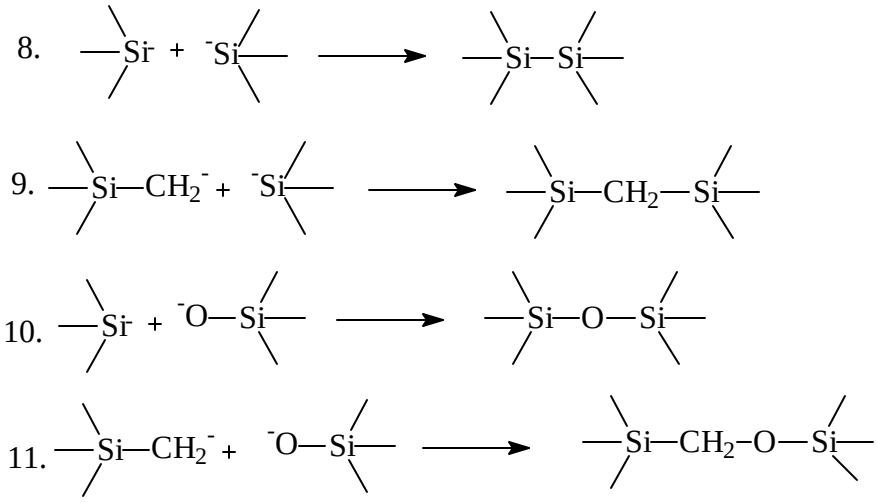

Table I. Density and porosity of SiCOH films.

Dielectric constant	Density (g/cm^3)	Porosity Fraction	Pore diameter (nm)
2.80	1.32	0	N/A
2.40	1.06	0.20	< 1.5
2.05	0.87	0.29	< 2.5

Table II. FTIR peak assignments. Major contributors are listed first for each vibration. n**=stretching,** d=**bending,** r=**rocking, a=antisymmetric, s=symmetric.**

TMCTS	k=2.8	k=2.05	Mode	Comment	References
2968	2969	2968	ν^a C-H_3	sp^3 CH_3	15-18, 32
2906			ν^s C-H_3	sp^3 CH_3	15-18, 32
	2916	2932	ν^a C-H_2	sp^3 CH_2	15-18, 32
	2880	2875	ν^s C-H_2	sp^3 CH_2	15-18, 32
	2232		ν^s Si-H	H-SiO_3	8-14
	2178		ν^s Si-H	H-SiO_2Si	8
2165			ν^s Si-H	H-SiOSi	8
		1740, 1714	ν C=O	As deposited only	15
		1461	δ C-H_2	CH_2 isolated from Si	15, 35
1405	1412	1412	δ^a C-H_3	$SiMe_x$	15-19, 32
	1358	1379	δ C-H_2	Si-CH_2-Si	15-19
1259	1273	1274	δ^s C-H_3	$SiMe_x$	15-19, 26, 32, 36
	1135	1140	ν^a Si-O-Si ν C-O	Cage Si-O-Si angle ~150° Si-O-C	9-10 11-13, 20 16, 24, 25
1063	1063	1065	ν^a Si-O-Si	Network (network) Si-O-Si angle ~144°	9, 10
	1023	1035	ν^a Si-O-Si	Silicon suboxide, Si-O-Si angle <144° D_{3h} ring structure	21, 22, 23 16, 17
	890		δ H-Si-O ν Si-C, ρ^s CH_3	H-SiO_3 $SiMe_2$	8-14 15-18, 19, 24, 33
865			δ H-Si-O	H-SiO_2Si	8
	848	843	δ H-Si-O ν Si-C, ρ^a CH_3	Network smaller angle $SiMe_3$	10, 12-14, 35 15-19, 24, 26, 33
	802	800	ν Si-C, ρ^a CH_3	$SiMe_2$	15-19, 24, 33
754			ν Si-C, ρ Si-CH_3	$SiMe_1$	
	773	779	ν Si-C, ρ CH_3 ν Si-C, ρ^s CH_3	$SiMe_1$ $SiMe_3$	18, 24, 36 15-19, 24, 33
710	730	720	ν^s Si-O-Si		11, 12, 13
	440	440	δ of O-Si-O	Network and ring opening vibrations	11, 12, 13

Table III. Integrated peak areas for TMCTS and annealed SiCOH films.

Vibration	Region integrated cm^{-1}	TMCTS	k=2.8	k=2.5	k=2.27	k=2.05
C-H_x	3100-2800	1.24	0.67	3.88	2.47	2.36
Si-H	2400-2000	13.29	1.72	0.10	0	0
CH_2 (Si free)	1550-1425	0	0	0.2	0.1	0.06
Si-CH_3	1300-1250	4.59	0.95	0.81	0.65	0.70
Si-O-Si	1250-950	65.5	29.7	28.2	18.1	20.1
H-Si-O	890	67.0	2.35	0.59	0.20	0.09
H-Si-O, $SiMe_3$	848	n/o	3.07	1.41	1.22	1.02
$SiMe_2$	802	n/o	1.98	1.28	0.48	0.36
$SiMe_1$, $SiMe_3$	778	53.4	2.07	0.91	0.98	1.01

Table IV. Bond strengths of diatomic molecules [27]

Bond	Energy (kJ mol^{-1})	Bond	Energy (kJ mol^{-1})
C-O	1076	Si-O	800
C-C	610	Si-C	451
C-H	338	Si-H	$\leq$299
		Si-Si	325

Figure captions

Figure 1: Dielectric constants of SiCOH films vs. CH2./TMCTS ratio in the gas feed

Figure 2: Elemental concentration ratios vs. CH2/TMCTS ratio in the gas feed for as deposited and annealed SiCOH films.

Figure 3. FTIR spectra of (a) TMCTS monomer; (b) annealed SiCOH film grown from TMCTS only (k=2.8); (c) as deposited and (d) annealed SiCOH film grown from TMCTS with organic precursor (k=2.05).

Figure 4: Deconvolution of the Si-O-Si absorption band of SiCOH films. a) k=2.8; b) k=2.05.

Figure 5: Deconvolution of the SiMe and HSiO absorption bands of SiCOH films. a) k=2.8; b) k=2.05.

Figure 6. Peak area ratios of FTIR absorption of (a) CH_i (3100-2800 cm^{-1}), (b) H-Si-O and $SiMe_2$ (890 cm^{-1}), (c) H-Si-O and $SiMe_3$ (848 cm^{-1}), (d) $SiMe_2$ (802 cm^{-1}), (e) $SiMe_1$ (775 cm^{-1}), and (f) Si-H (2400-2000 cm^{-1}) to the area of the $SiCH_3$ absorption (1275 cm^{-1}) in annealed SiCOH films.

Figure 7. Area ratios of the deconvoluted oxide peaks vs the dielectric constant of the SiCOH films.

Figure 8. FWHM of the deconvoluted oxide peaks vs the dielectric constant of the SiCOH films.

Figure 9. Diagram of networked structure of annealed SiCOH film deposited from TMCTS only.

Figure 10. Diagram of porous cage networked structure of annealed SiCOH film deposited from TMCTS with organic precursor.

Figure 11. Variation of Si-O-Si bonding angle.

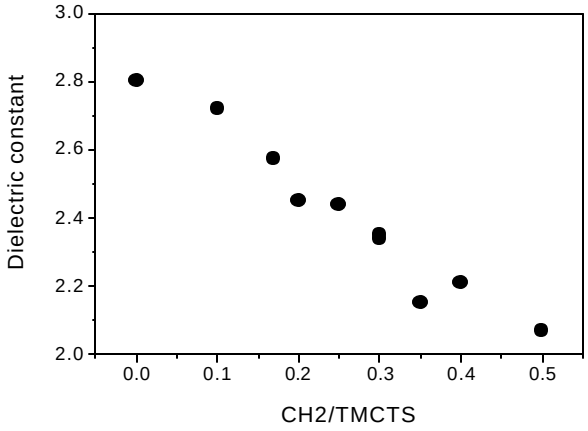

Figure 1: Dielectric constants of SiCOH films vs. CH2./TMCTS ratio in the gas feed

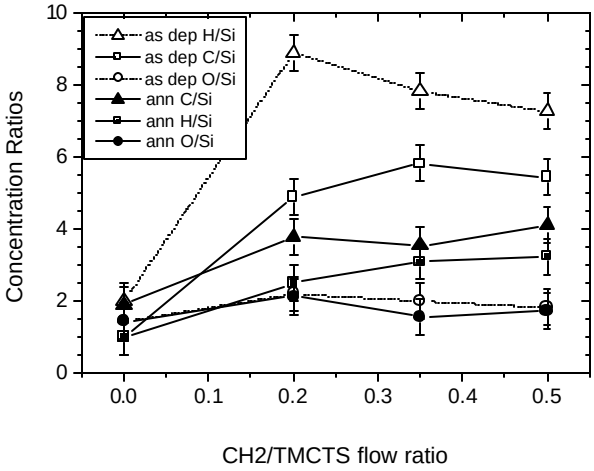

Figure 2: Elemental concentration ratios vs. CH2/TMCTS ratio in the gas feed for as deposited and annealed SiCOH films.

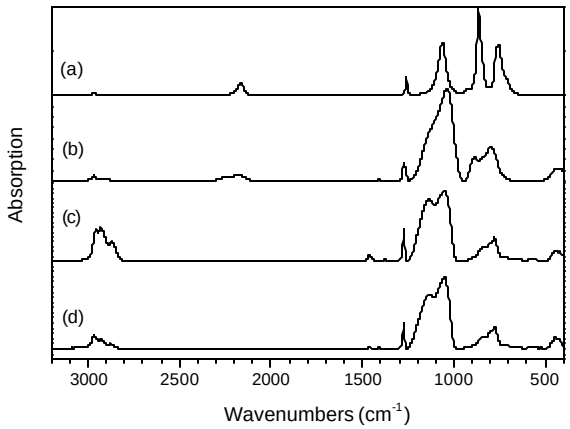

Figure 3. FTIR spectra of (a) TMCTS monomer; (b) annealed SiCOH film grown from TMCTS only (k=2.8); (c) as deposited and (d) annealed SiCOH film grown from TMCTS with organic precursor (k=2.05).

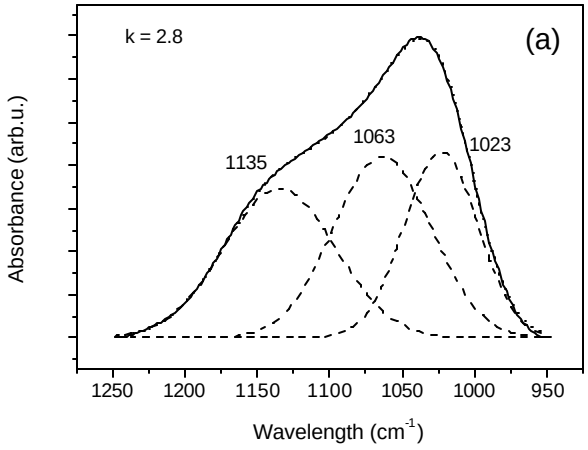

Figure 4a: Deconvolution of the Si-O-Si absorption band of SiCOH films. a) k=2.8; b) k=2.05.

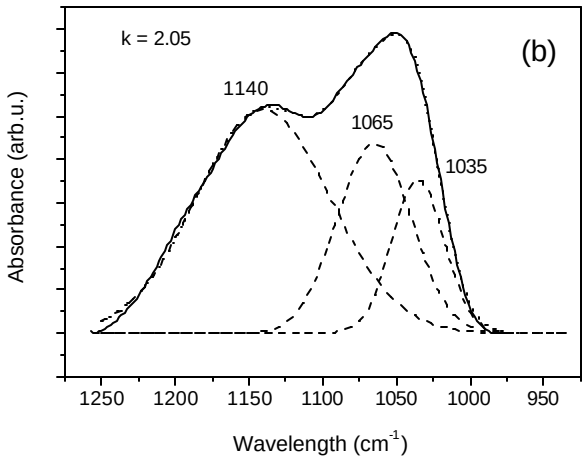

Figure 4b: Deconvolution of the Si-O-Si absorption band of SiCOH films. a) k=2.8; b) k=2.05.

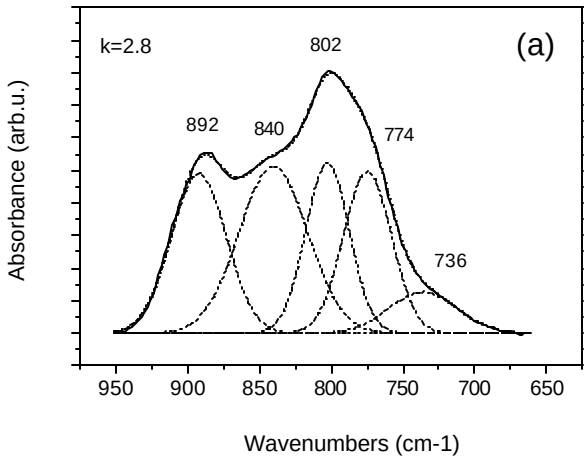

Figure 5a: Deconvolution of the SiMe and HSiO absorption bands of SiCOH films. a) k=2.8; b) k=2.05.

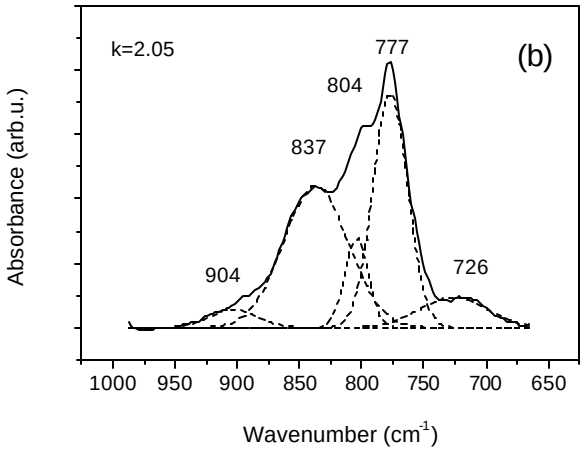

Figure 5b: Deconvolution of the SiMe and HSiO absorption bands of SiCOH films. a) k=2.8; b) k=2.05.

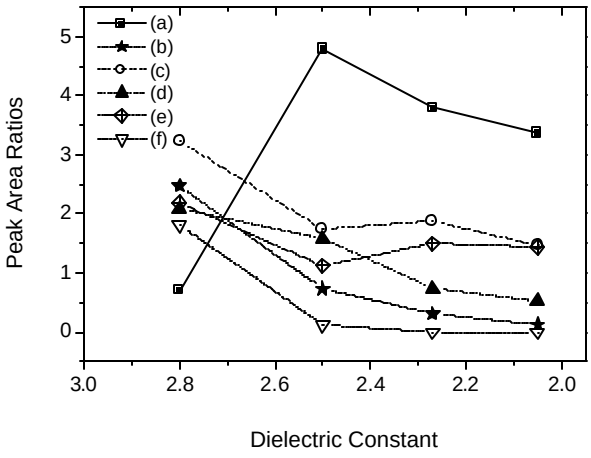

Figure 6. Peak area ratios of FTIR absorption of (a) CH_i (3100-2800 cm^{-1}), (b) H-Si-O and $SiMe_2$ (890 cm^{-1}), (c) H-Si-O and $SiMe_3$ (848 cm^{-1}), (d) $SiMe_2$ (802 cm^{-1}), (e) $SiMe_1$ (775 cm^{-1}), and (f) Si-H (2400-2000 cm^{-1}) to the area of the $SiCH_3$ absorption (1275 cm^{-1}) in annealed SiCOH films.

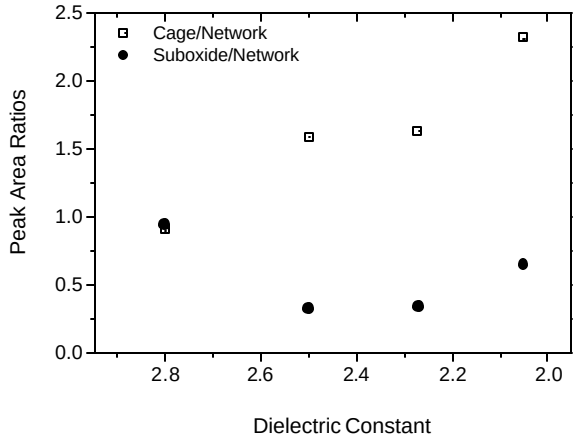

Figure 7. Area ratios of the deconvoluted oxide peaks vs the dielectric constant of the SiCOH films.

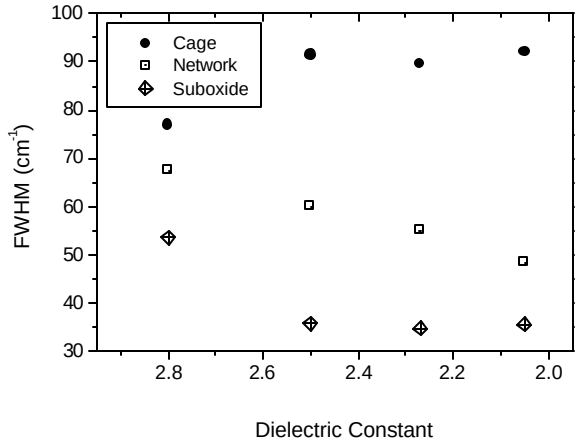

Figure 8. FWHM of the deconvoluted oxide peaks vs the dielectric constant of the SiCOH films.

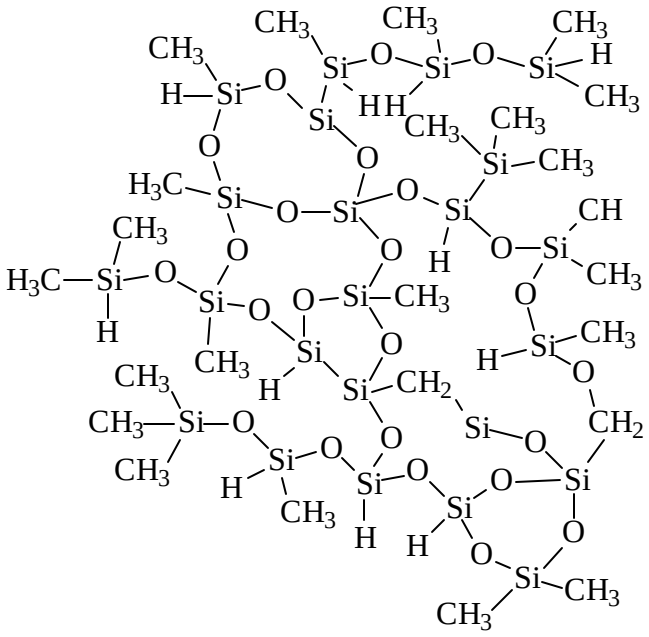

Figure 9. Diagram of networked structure of annealed SiCOH film deposited from TMCTS only.

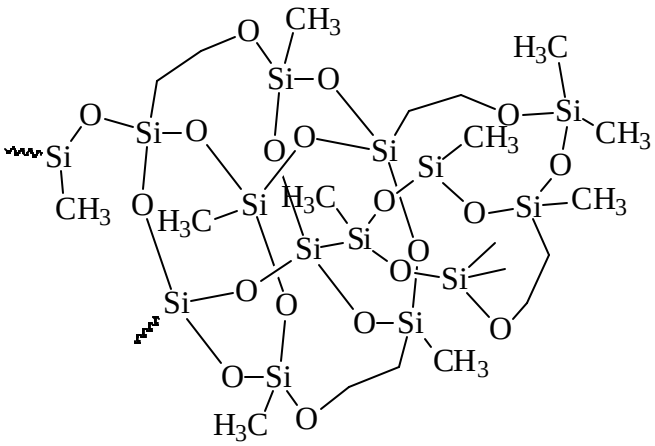

Figure 10. Diagram of porous cage networked structure of annealed SiCOH film deposited from TMCTS with organic precursor.

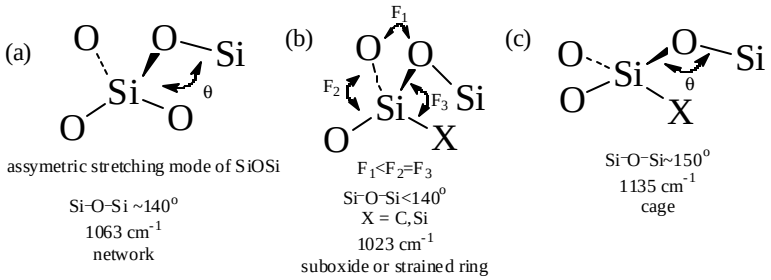

Figure 11. Variation of Si-O-Si bonding angle